Communications Research Centre

LEVEL II

(3)

B-3

AN INVESTIGATION OF HF DIRECTION-FINDING ACCURACY ON THE FROBISHER BAY-OTTAWA AURORAL ZONE PATH

by

G.O. Venier

This work was sponsored by the Department of National Defence, Research and Development Branch under Project No. 33G00

DEPARTMENT OF COMMUNICATIONS
MINISTÈRE DES COMMUNICATIONS

CRC TECHNICAL NOTE NO. 703

CANADA

OTTAWA, JULY 1980

(14) CRC-TTN-703

COMMUNICATIONS RESEARCH CENTRE

DEPARTMENT OF COMMUNICATIONS
CANADA

(6) AN INVESTIGATION OF HF DIRECTION-FINDING ACCURACY ON THE FROBISHER BAY–OTTAWA AURORAL ZONE PATH

by

(10) G.O. Venier

(Radio and Radar Research Branch)

(12) 40

(9) CRC TECHNICAL NOTE NO. 703

(11) July 1980
OTTAWA

This work was sponsored by the Department of National Defence, Research and Development Branch under Project No. 33G00

4041-11 9W

TABLE OF CONTENTS

AN INVESTIGATION OF HF DIRECTION-FINDING ACCURACY ON THE FROBISHER BAY-OTTAWA AURORAL ZONE PATH

by

G.O. Venier

ABSTRACT

The CRC HF direction-finding array, consisting of a 1181 meter by 236 meter cross, was used to make angle of arrival measurements of waves transmitted over a 2100 km path whose mid point was near the centre of the auroral zone. Swept-frequency transmissions allowed the investigation of the angle variations of individual propagation modes, and fixed-frequency transmissions permitted the measurement of Doppler shifts as well as the sampling of the phase fronts at relatively high rates.

E-mode propagation over this path appeared to be entirely of the sporadic variety, but still provided good azimuth accuracy with a median RMS error from the great circle direction around 0.4 degrees for the single-hop case. On the F mode, spreading in range occurred a significant percentage of the time in contrast to experience with lower-latitude paths. This spreading was accompanied by large departures in angle of arrival for this mode from the great circle direction.

Two azimuth-estimation techniques were tested on the fixed-frequency data. One used a phase-front planarity test and averaging over relatively frequent samples while the other was based on the separation of modes by Doppler processing. The former technique was found to provide slightly better results than the latter on these data, and its accuracy was, in most cases, close to that which could be obtained from the best mode when separated using swept frequency data.

1. INTRODUCTION

The CRC high-frequency direction-finding array has been used in a number of experiments intended to determine the characteristics of errors in direction estimates caused by propagation via the ionosphere. In the experiment described here, the transmitter was situated at Frobisher Bay at about 64°N latitude at a distance of just over 2100 km from the receiving system near Ottawa. This meant that the propagation path was through the auroral zone with the mid-point not far from the centre of the zone. Propagation conditions along such a path were expected to be more disturbed than those for the lower-latitude paths. The purpose of the experiment was to investigate the characteristics of these conditions, and to determine their effect on the accuracy of high-frequency direction-finding systems.

A ranging capability in the transmitter-receiver system allowed the separation and identification of various propagation modes so that each could be studied without interference from the others, and a high level of coherency in the system allowed the measurement of Doppler shift with high accuracy and resolution (the range and Doppler frequency capabilities could not be used simultaneously). Finally, the large aperture of the array provided the capability of sampling phase fronts over a large spatial extent.

The results to be presented here include the following:

(a) the azimuth-error statistics of the various propagation modes,

(b) the statistics of azimuth-estimate errors for a measurement technique using averaging of azimuths computed from individual scans across the antenna elements, with a phase-front planarity test to discard unsuitable scans from the average,

(c) the error statistics of an azimuth-estimation scheme in which a weighted mean of azimuths of Doppler-separated modes is computed. The weights depend on parameters related to the expected accuracy of the modes, and

(d) a more detailed examination of the mode which is perhaps most characteristic of auroral-zone propagation, range-spread F.

2. DESCRIPTION OF EXPERIMENT

A description of the CRC high-frequency direction-finding system can be found in reference 1, but some of the important characteristics are included here. The antenna configuration used is shown in Figure 1.

Much better resolution in angle is possible from the longer array. In most experiments to date the transmitter has been located in a direction either nearly normal to this array, for good azimuth resolution, or, nearly in line with it for good elevation-angle resolution. In this experiment the direction to the transmitter was about half way between the two array axes, and azimuth and elevation angle measurements each depended on both arrays.

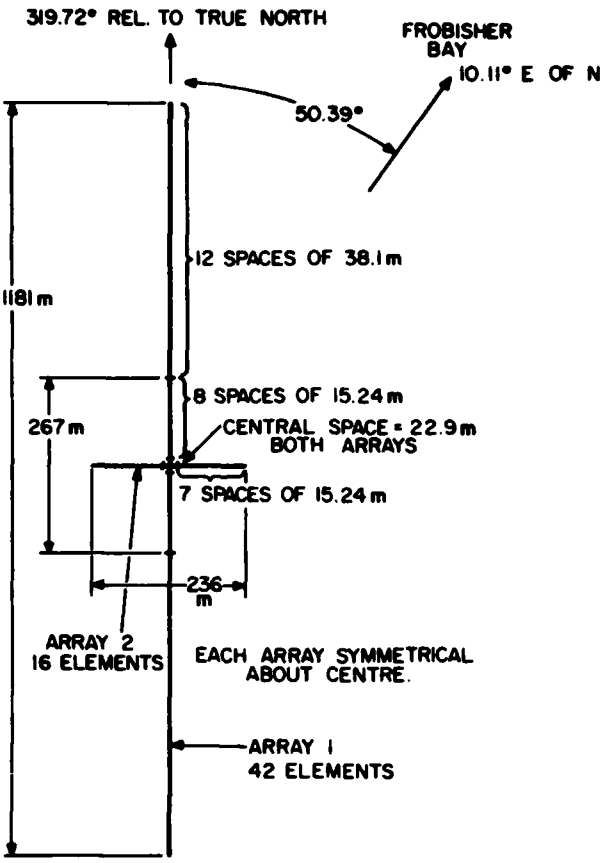

Figure 1. Antenna Configuration

There were 42 elements in array 1 and 16 in array 2, a total of 58, each feeding its own receiver. These were scanned sequentially, and in-phase and quadrature (I and Q) samples with respect to a reference receiver were digitized to 12 bits and recorded for each antenna on each scan. The AGC level of each receiver was also recorded to allow amplitude correction. The signal was heterodyned down to essentially zero frequency before sampling resulting in both positive and negative frequency components in the tens of Hertz range. Phase errors caused by the time required to scan the receivers sequentially were corrected when the recorded signal was later processed.

Two types of transmission were used in this experiment: a fixed-frequency signal with a duration of five seconds, and a swept-frequency signal sweeping through 100 kHz in one second. These signals were transmitted once per minute, the fixed-frequency signal starting 20 seconds after the beginning of the swept frequency signal. The sampling rates were 128 array scans per second for the swept frequency and 51.2 scans per second for the fixed frequency. The time required for each scan of the array was about three milli-seconds. Rubidium-vapour frequency standards were used in both the transmitter and receiver to provide accurate timing and coherence.

Every 20 minutes, the above transmissions were stopped for about 4 minutes during which time the transmitter sent a long frequency sweep and the receiving-and-data system processed it to produce an oblique ionogram. These were used to help select frequencies for transmission and also, in the later analysis, to identify the propagation modes present. Larger gaps (8 minutes) in the data occurred once per hour when it was necessary to change tapes.

The transmitting antenna at Frobisher Bay had coordinates of 63° 43' 27" N latitude and 68° 26' 50" W longitude, and those of the CRC HFDF receiving array near Ottawa are 45° 13' 38" N and 75° 50' 57" W. This gave an azimuth for the transmitter as seen from the HFDF site of 10.11 degrees E of N and a ground distance of 2107.8 km. The latitude of the mid-point was about 54.5° N, which is near the centre of the auroral zone.

The experiment was carried out over a two week period from November 24 to December 7, 1976. Measurements were made over 12 hour periods extending from noon to midnight the first week and from midnight to noon the second week.

3. METHOD OF ANALYSIS

3.1 FIXED-FREQUENCY DATA

The fixed-frequency operation was included in the experiment to allow the investigation of the Doppler characteristics imparted to the signals by the ionosphere and also to allow a study of the short-term characteristics as found from a scan-by-scan analysis of the data. To obtain frequency spectra, the five-second data intervals recorded from each receiver were cosine-squared preweighted and then Fourier transformed. A complex transform was performed on the I- and Q-channel data over the 256 samples (51.2 samples per second over 5 seconds). An offset of 12 Hz was used between the transmitter and receiver frequencies to prevent the zero Doppler shift occurring at zero frequency where the receiver introduces additional noise. The resulting 256 complex numbers for each receiver, representing the amplitude and phase of the signal for 256 Doppler shifts uniformly spaced over a 51.2 Hz window, were recorded on a secondary magnetic tape for later stages of the analysis. Since the phase of the signal at each receiver was retained, the direction of arrival could be determined from the relative phases across the array of receivers. Further, this direction-finding process could be carried out independently for each of the 256 Doppler cells. Therefore, if two or more modes were received with different Doppler shifts, the direction of arrival of each could be determined.

3.1.1 Analysis of Doppler-Processed Tapes

The data, after processing for Doppler shift as described in Section 3.1, may be used as input to a number of programs. One of these programs, referred to here as DOPSPD, computes the Doppler spread on the signal as a function of time; that is, it computes and displays a Doppler-spread value for each 5-second transmission. Doppler spread is defined here as twice the standard deviation of the Doppler shift where each Doppler shift is weighted by the power in that cell. That is, Doppler spread is

$$f_{ds} = 2 \times \left(\sum_{i=1}^{256} P_i \cdot (f_{di} - f_{dm})^2 / \sum_{i=1}^{256} P_i \right)^{\frac{1}{2}}$$

where P_i is the power in the i^{th} Doppler cell
f_{di} is the Doppler frequency corresponding to the i^{th} cell and
f_{dm} is the mean Doppler frequency, weighted by power; i.e.

$$f_{dm} = \sum_{i-1}^{256} P_i \cdot f_{di} / \sum_{i=1}^{256} P_i .$$

The Doppler spread, f_{ds}, is corrected for the effect of broadening by the window function. The Doppler spread is a measure of the rate at which we might expect changes to occur in the phase fronts when the modes have not been separated.

A second program referred to here as AZEL3 computes the azimuth and elevation of each of the ten Doppler cells with the highest amplitude. Cone angles for the signal in each Doppler cell are first computed for each of the arrays by means of a linear least-squares fit to the phases across the array. Cone angle is defined here as the angle between the line of the array and the normal to the phase front, since, for a linear array, the possible directions of arrival which make this angle with the array fall on the surface of a cone. Azimuth and elevation are determined by solving for the intersection of the cones for the two arrays. For each of the least-squares lines computed, the RMS deviation of the phases at each element from this straight line is also computed. The larger this number, which will be referred to here as the RMS phase deviation, the more distorted (from planar) the phase front must be. Since distortions in the phase front result from wave interference[2,3] and generally result in bearing errors, the RMS phase deviation may be used as an indication of the quality of the measurement. Program AZEL3 prints out the computed azimuth, elevation, RMS phase deviations, power, radio frequency and Doppler frequency for each of the ten Doppler cells mentioned above.

One method of improving azimuth estimates by making use of the Doppler-processed data is referred to here as the weighted mean method. This method forms a weighted mean of the azimuths using the Doppler cells with the greatest amplitudes. The method is described in more detail in reference 4 but a general description is included here.

For each of the 8 Doppler cells containing the largest amplitude signal (the number 8 is a parameter in the program which may be changed), the azimuth and elevation are computed by the least squares fit method described earlier. The azimuth is given a weight which depends on RMS phase deviation across the array, and on elevation angle and received power. The weight increases with decreasing RMS deviation, decreasing elevation angle and increasing power. A weighted mean is then computed from the azimuths from

each cell, and this is taken as the azimuth estimate. An overall weight, indicating the quality of the azimuth estimate, is also computed (this was not indicated in the above reference) and can be used in a decision as to whether or not to accept the result. The overall weight is computed from the sum of the cell weights multiplied by a Doppler-spread weight and a bearing-spread weight. These last two are computed from the standard deviation of Doppler and bearing across the cells used. Large spreads on Doppler and azimuth are an indication of poor conditions resulting either from the propagation medium or interference, and result in a low overall weight.

The formulas and parameters used in computing the weights for this experiment are given in the Appendix. The parameters were chosen on the basis of experience with data from a shorter, lower-latitude path. They probably are not optimum for the path of this experiment.

3.1.2 Scan-by-Scan Analysis of Fixed-Frequency Data

In the Doppler-processed data, only one phase is available from each Doppler cell for each antenna element. This phase represents an average over the full five-second recording time. In this Section we consider the analysis of the signal in the time domain on a scan-by-scan basis; that is we look at the phase of each element for each scan of the array.

The antennas elements are sampled sequentially within a scan, and the resulting time delay between element samples produces phase errors. Such errors are frequency dependent, and the corrections are applied in the frequency domain. For this reason, the scan-by-scan data were regenerated by an inverse Fourier transform on the corrected Doppler data. Sample-and-hold amplifiers have since been installed in the system to make the sampling simultaneous, and these corrections will not be necessary in the future.

Since it was assumed that the correlation time of the phase-front distortions was much longer than 0.02 seconds (approximately the inverse of the scan rate), and that signals did not exist outside the Doppler frequency range of $\pm$ 6.4Hz, only one quarter of the Doppler cells, centered about zero Doppler, were transformed back to the time domain. This resulted in only 64 uniformly spaced time samples over the 5-second period. That is, the effect was to reduce the scan rate by a factor of four. These data allowed us to look at the phase, and hence angle of arrival, every 0.078 seconds.

Actually only 63 samples were used since the cosine-squared pre-weighting on the original data had the effect of reducing the resultant values at each end of the time window to the levels where quantization errors were significant; the first value was generally below the quantization level and was discarded. Quantization noise on some of the remaining samples may have had a small effect on the results.

The linear least-squares fit method was used, as with the Doppler processed data, to determine azimuth, elevation angle, and RMS phase deviations for each of the 63 scans. These were used in a simple azimuth-estimation scheme based on averaging azimuth results over the 63 scans, and on testing for low RMS phase deviation as a criterion for including the azimuth from the scan in question in the average. It was assumed that a high RMS phase deviation is an indication of a probable large error.

In the choice of threshold levels for RMS phase deviation, we wish to use an optimum threshold which will keep the single-scan error low, and yet allow enough scans to pass the test to provide a good average. The RMS phase-deviation thresholds used in this analysis were 80 degrees for array 1 and 15 degrees for array 2. These were chosen on the basis of a statistical study of the data which will be reported elsewhere.

It is of course recognized that for scans taken a short time apart, there will likely be considerable correlation in the phase linearity and also in the angle errors. That is, the angle samples are not all independent, and averaging of a given number of scans will not reduce the error by the factor expected for independent samples. The correlation time of the wave-front shape has been investigated in reference 3. It will be sufficient here to note that the correlation time is on the order of one second. When modulated signals are received this correlation time can be considerably less, as a result of the effect of the modulation on the interference between two or more modes[5]. Further work is required to determine whether this will actually allow more independent samples to be averaged in a given time.

A program called AZPLT6 computes azimuth estimates as described above, and plots the results. One estimate is produced each minute for the five seconds of data.

AZPLT6 also computes the RMS error from the true azimuth, of the averaged result over any desired interval (roughly 30 minute intervals were used in this study). Results can be witheld from the RMS-error calculation if a specified number of scans did not pass the RMS phase-deviation test and were not included in the five-second average. A criterion of 20 out of 63 scans, for inclusion in the statistics, was used in analyzing the results presented here.

3.2 SWEPT-FREQUENCY DATA

Swept frequency signals were transmitted to allow separation of propagation modes on the basis of path length, or range. The received signal was heterodyned with a replica of the transmitted signal, giving an output whose frequency was proportional to range. The 100 kHz sweep used provided a range resolution of about 10 microseconds. The scan rate was 128 scans per second in this experiment, providing 128 samples per channel in the one-second transmission time. This resulted in a range window of 1.28 milliseconds which could be centered at any desired range by control of the delay between the transmitted waveform and the replica used for heterodyning.

Analysis of the swept-frequency data is essentially the same as that of the fixed-frequency data. Where a spectral analysis of the latter provides Doppler information, a spectral analysis of the swept-frequency data provides range information as a result of the correspondence between range and frequency after heterodyning. Thus the first stage of processing is a discrete Fourier transform as before. The result is 128 range cells for each receiver, again with complex data, allowing the phase for each receiver at each range to be determined. These are recorded on a secondary magnetic tape which is used as input for other analysis routines.

One such routine provides a display of the amplitude, averaged over all receivers, for each range cell, as a function of time (one per minute). Range and time form the two spatial dimensions of the plot and the amplitude is coded as a character, providing a kind of contour plot. Modes can be identified on these plots by comparison with the ionograms, and the plots provide a history of the ranges for the various modes between ionograms. The plots are used to select range windows corresponding to individual modes for further analysis.

A program called AZEL1 which is similar to AZEL3 computes the same values as AZEL3, except that Doppler frequency is replaced by range.

Program AZPLT5 produces an output of azimuth and elevation as a function of time for a selected range window. It computes the azimuth and elevation for the range cell with the greatest amplitude within this window, using the linear least-squares fit method. If the elevation falls within specified limits and the RMS phase deviation is below a specified value, the computed azimuth is included in a long term average of RMS error which is computed over specified intervals, usually about 30 minutes. If the elevation and RMS phase-deviation criteria are not satisfied, the range cell with the next highest amplitude is tried, until the criteria are satisfied or ten ranges have been tried.

The range window is used to select a particular mode and the RMS-phase-deviation and elevation-angle criteria help to discriminate against interference and ambiguities. Thus the result should be a good measure of the best azimuth estimate which can be made for the one-second signal when the propagation occurs in only one mode. This is intended first as a means of comparing the potential of different modes for azimuth estimates, and secondly, as a reference against which to test possible operational techniques which cannot make use of range to separate modes.

4. EXPERIMENTAL RESULTS

4.1 AZIMUTH ERROR STATISTICS

4.1.1 Range-Separated Modes

Figures 2 and 3 show the modes that were present throughout the experiment at the operating frequency of the system which is recorded near the bottom of the figure. Figures 2 and 3 are only rough indications taken from the ionograms. The F mode was called spread F if the range extent was about 0.1 millisecond or greater. The points marked MUF are times when the maximum frequency for the F mode was in the process of dropping below the operating frequency. Large errors are generally expected near such times.

Most of the swept-frequency data were analyzed by AZPLT5 for each of the modes present at the time to produce plots of the azimuth as a function of time, and RMS errors in azimuth measured over approximately 30 minute periods. Data where interference was evident, or where the signal was very weak, or near the MUF, were discarded. An RMS phase-deviation criterion of

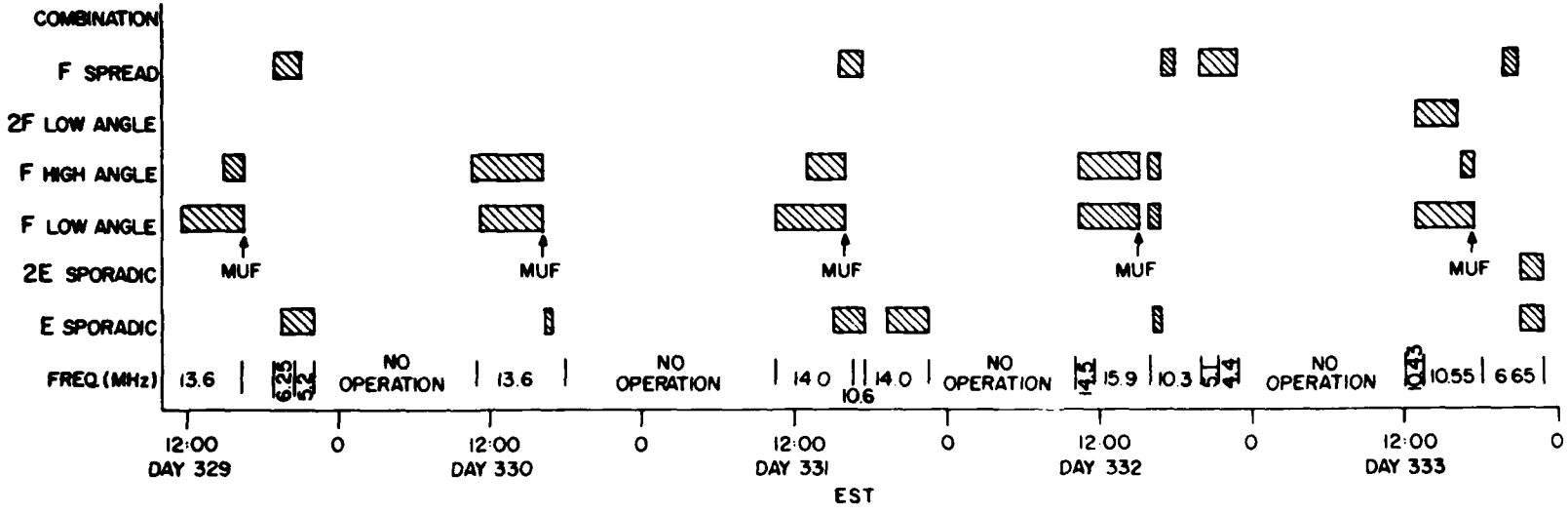

Figure 2. Modes Present at Operating Frequency
Days 329 to 333

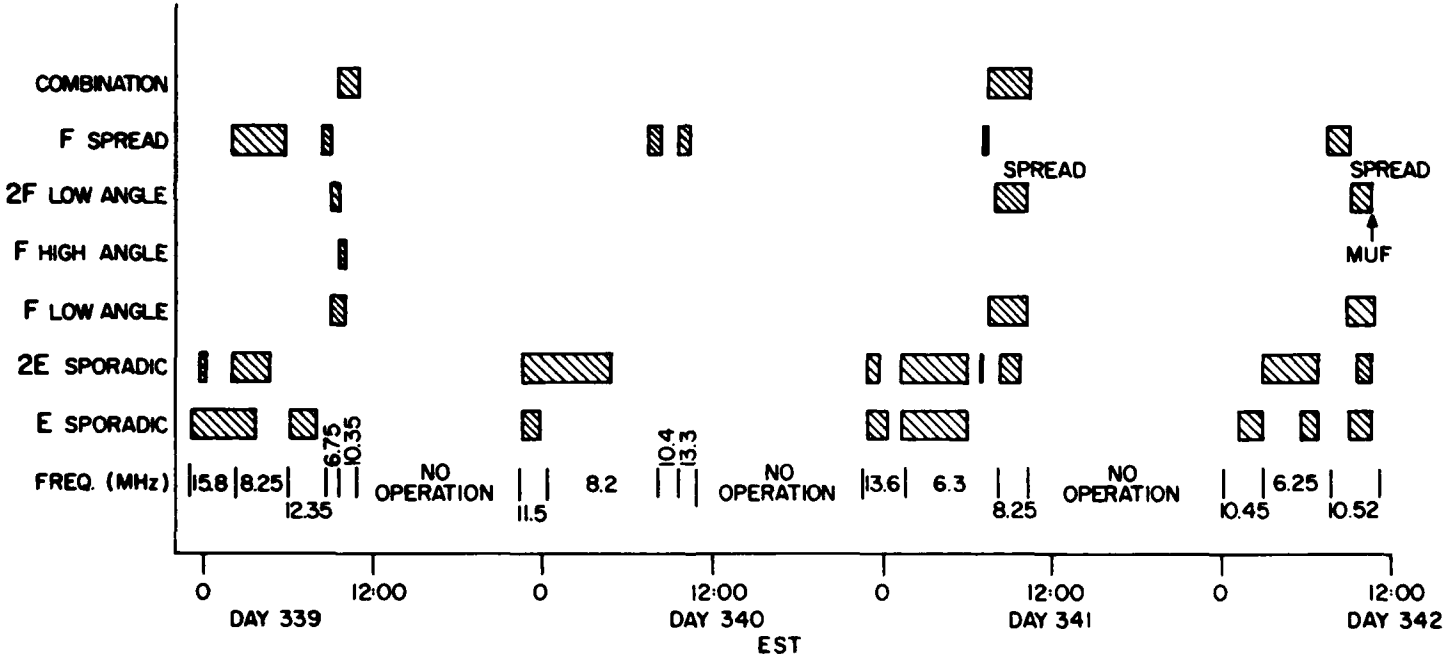

Figure 3. Modes Present at Operating Frequency
Days 338 to 342

40 degrees on array 1 and 20 degrees on array 2 was used. These values were selected from experience to remove most poor phase fronts while not rejecting too many good ones. The results were then analyzed in two ways.

First, time segments over which various conditions persisted were chosen. For each time segment a histogram was drawn of the azimuth estimate for each one-minute interval (one second of data). These were done for time periods of from less than an hour to a few hours. Examples are shown in Figures 4 to 9. These are intended to be typical. The range of errors found for each mode will be discussed later.

Figure 4 is a typical histogram for the Sporadic E mode. It has an RMS error, from the true azimuth of 10.11 degrees, of only 0.38 degrees. This histogram is for a roughly two-hour period around midnight EST. Of the 90 azimuth estimates available over this period, only 63 satisfied the rms-phase-deviation criterion and were used in the histogram.

Figure 5 is a histogram of azimuths for a two-hop E mode over a period of just over one hour. The RMS error of 0.72 degrees is possibly a little lower than average for this mode, and the two occurrences which can be seen with fairly large error indicate that there is a potential for relatively large errors.

Histograms for low-angle F-mode azimuths are shown in Figure 6. The upper histogram is typical for normal, stable, F-mode conditions. The RMS error is only 0.59 degrees. The data for the lower histogram were recorded when spread-F conditions prevailed, in this case after sunset. The ionogram showed great spread in range (up to about 0.5 milliseconds) with no real high and low-angle structure in evidence. As can be seen, azimuths are spread over a wide angle and the RMS error is very high. The contrast between the errors for the normal and the spread conditions is great. These spread conditions occur reasonably often on this Frobisher-Ottawa Path as can be seen from Figures 2 and 3, and can be expected to seriously degrade direction-finding accuracy.

Figure 7 shows histograms for high-angle F-mode propagation, again for normal and spread conditions. The upper histogram for normal good conditions indicates reasonably low errors, with an RMS value of 0.65 degrees. The lower histogram shows the errors for a case where the high-angle trace was somewhat spread (up to about 0.15 milliseconds) but where the ionogram clearly showed low and high-angle traces. Although the range spread was much less than that in the previous example the results are about as bad, with an RMS error of 3.44 degrees.

A few cases of two-hop low-angle F mode were recorded. Two examples are shown in Figure 8, where the upper histogram represents probably better than average results for this mode over this path, and the lower represents poorer than average results. The latter measurement was done not far from the maximum frequency of the two-hop propagation, and some spread in range was evident. It can be seen that the azimuth estimates from this latter measurement are heavily biased.

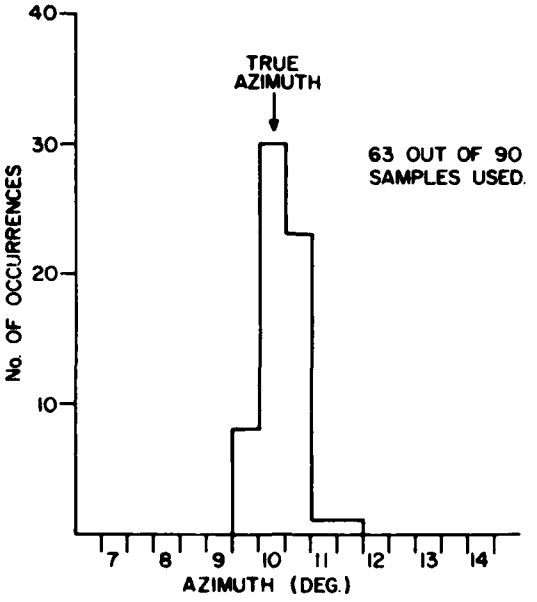

Figure 4. Histogram of Azimuth Estimates for Es Modes
Day 338 23:05 to Day 339 00:59

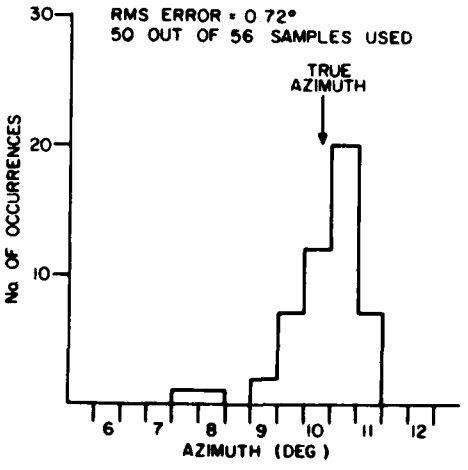

Figure 5. Histogram of Azimuth Estimates for 2Es Mode
Day 341 02:48 to 03:55

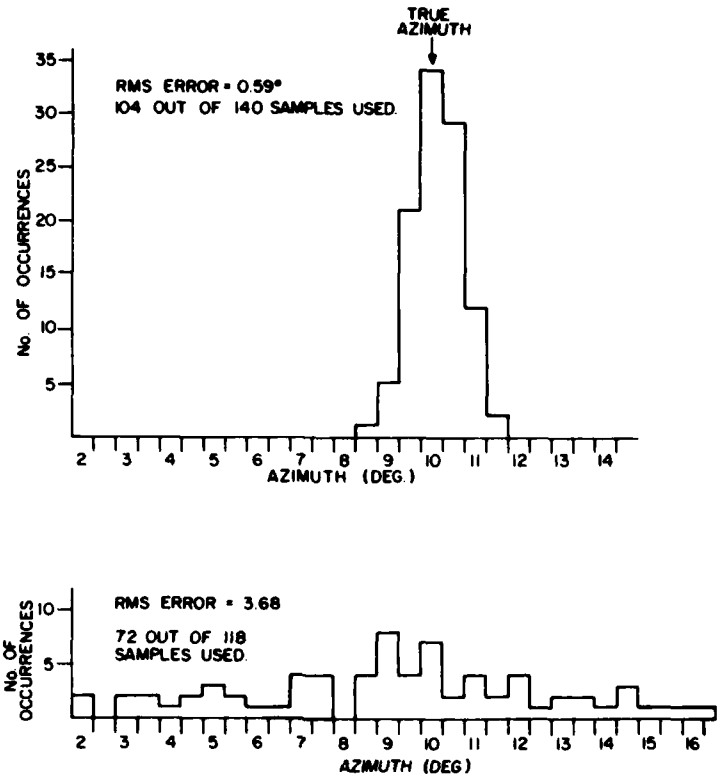

Figure 6. Histograms of Azimuth Estimates for Low-Angle F Mode
Upper Graph – Day 329 11:45 to 15:39, Normal F
Lower Graph – Day 332 20:04 to 22:35, Spread F

A few cases of combination modes (reflection from more than one layer and perhaps the ground as well) were recorded also. These showed wide variations in error, with the histogram of Figure 9 perhaps a typical one.

A view of the azimuth errors over the entire time of the experiment is presented in the histograms of Figure 10. For these histograms the data were analyzed in approximately 30-minute intervals. The individual measurements for each one-minute interval were used to determine the RMS error from the true azimuth. The resulting RMS errors, one for each 30-minute interval, were then used to produce the histogram. Again, data for periods where interference was evident, or where the operating frequency was very near the maximum useable for that mode, were discarded. Since each mode was present for only a part of the time of operation, the resulting number of good 30-minute intervals was not very large and some of the histograms are rather sparse. Still it is believed that these give a reasonable indication of the azimuth accuracy that can be expected from the various single modes.

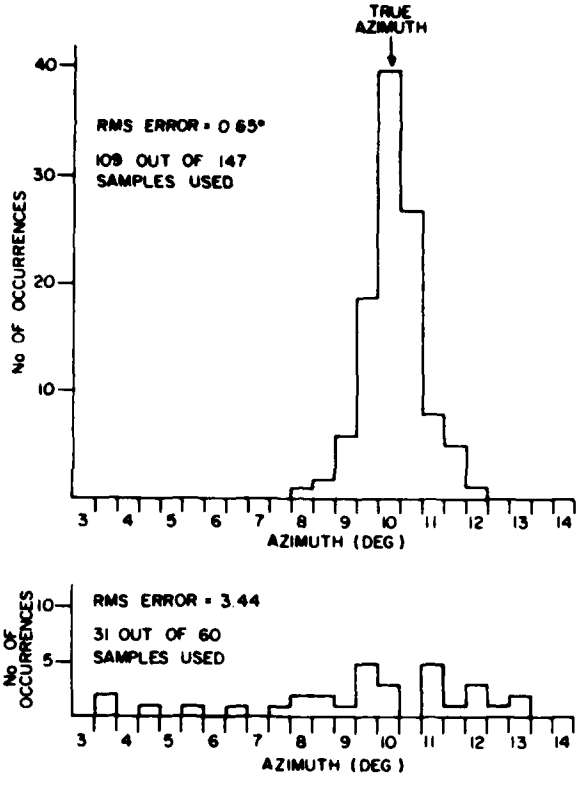

Figure 7. Histograms of Azimuth Estimates for High-Angle F Mode
Upper Graph – Day 332 11:45 to 14:59, Normal Conditions
Lower Graph – Day 333 16:04 to 17:19, Spread Conditions

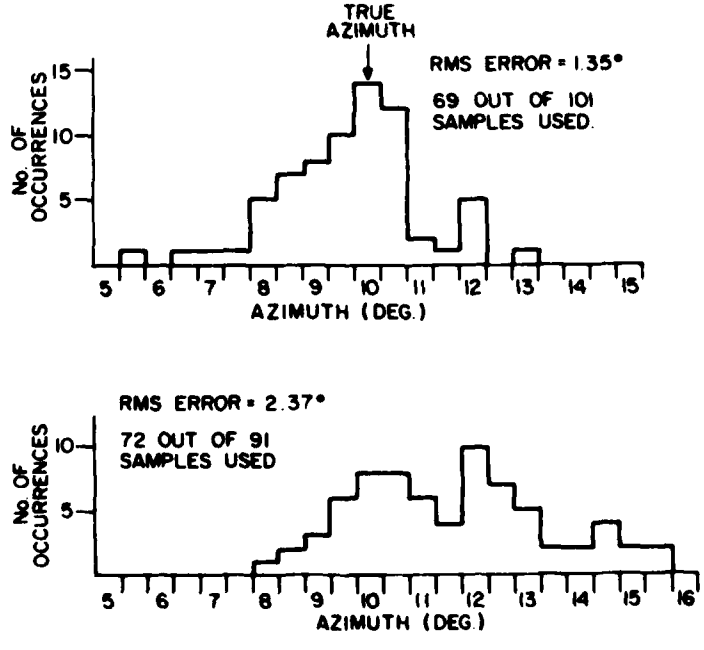

Figure 8. Histograms of Azimuth Estimates for 2-Hop Low-Angle F Mode
Upper Graph – Day 333 13:47 to 15:59
Lower Graph – Day 341 08:25 to 10:19

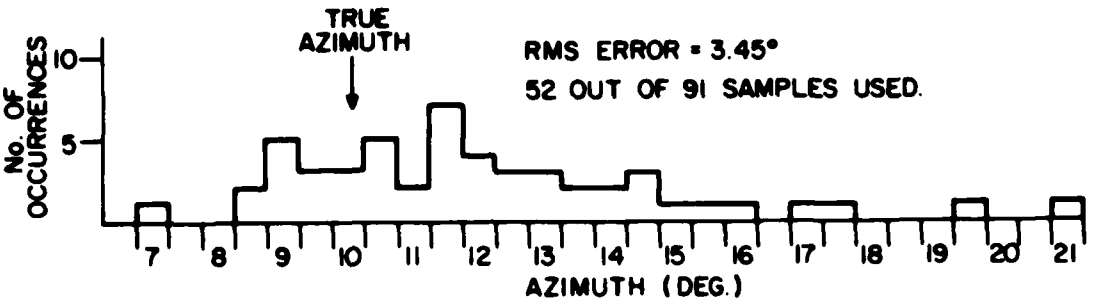

Figure 9. Histogram of Azimuth Estimates for Combination Mode Day 341 08:25 to 10:19

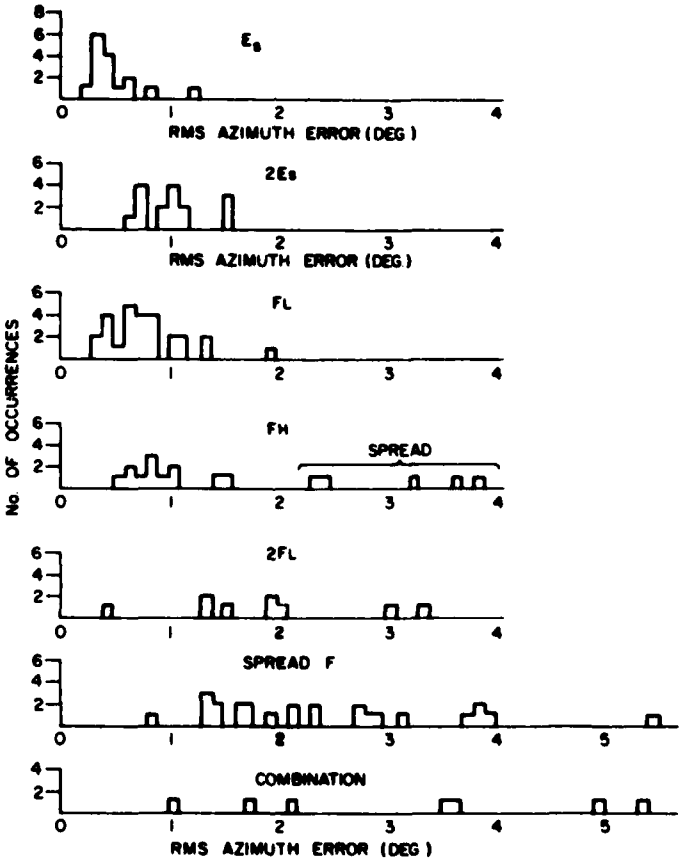

Figure 10. Histograms of RMS Azimuth Error for 30 Minute Averages

It is clear that the single-hop E mode returns give the best accuracy, even though they are a sporadic type of E and in some cases show considerable thickening or multiple apparent layers. The occurrences at 0.6, 0.8 and 1.2 degrees fit this latter category, and if these are removed the histogram indicates very high accuracy for the more "normal" sporadic E mode. As would be expected, the two-hop E_s-mode errors are somewhat higher than are the single-hop errors.

Low angle F-mode (FL) errors fall generally between those of the one and two-hop E_s errors, although for one 30-minute interval, the FL error was higher than the maximum 2-hop E_s error. Returns judged to be spread F were not included in the low-angle-F histogram but are presented separately. However, the division of the results into the two categories was somewhat arbitrary (a range spread of 0.1 milliseconds). The large-error result of about 1.9 degrees in the low-angle F histogram did have some spread in range, but not enough to satisfy the above criterion. The histogram for the returns considered to be spread F shows very large errors and a spread of errors from 0.8 degrees to 5.4 degrees. Included in this histogram are cases where the spread was great enough that high and low-angle traces were not visible on the ionograms. This would seem to be a very unreliable mode for direction finding.

High-angle-F errors are not much worse than the low-angle-F ones if the cases where spread occurred are ignored. These spread results were included in the same histogram in the high-angle case but are marked as such.

The few cases of two-hop F (low angle) do not indicate that this is a reliable mode for direction finding. Combination modes which may include M mode - two reflections from the F layer and one form from the top of the E layer - and N Mode - a two-hop mode with one reflection from each layer - show even poorer results.

Thus it appears that the single-hop E mode, even when sporadic, is by far the best mode for direction finding, while low-angle F mode would be a second choice if spread-F conditions can be avoided. Two-hop-E mode and high-angle F appear nearly as good as low-angle F. In the case of high-angle F however, spread conditions can cause serious errors.

Since spreading of F-layer returns seriously degrades their direction-finding potential, a question arises. Can the presence of spreading of F-layer returns be detected in an operational situation? Given enough time and a fixed transmitter, the variation in measured azimuths itself will be an indication. Also ionosondes give evidence of spread F, but will have to be situated so as to illuminate the area near the mid point of the path of interest. This is probably not feasible in an operational system, except for very limited search areas.

One parameter of the received signal which may be of use is its Doppler frequency and there is evidence that spread F conditions are generally accompanied by relatively large spreads in Doppler. This was investigated with the aid of the DOPSPD program described earlier. Mean values of Doppler spread were determined over the same time periods used for determination of RMS azimuth errors. A scatter plot was then drawn of Doppler spread against RMS azimuth error for low-angle-F and spread-F modes. Since these two modes

did not occur in the same intervals, the Doppler-spreads could be associated with the correct modes. In some cases, however, other modes occurred as well and may have had some effect on the Doppler spreads. The plot is shown in Figure 11. Most of the data included in the two relevant histograms of Figure 10 were used, although some were discarded due to poor estimates of Doppler spread. This plot clearly shows that the error in the spread-F estimates, identified by x's, was greater than that in the normal low-angle-F estimates, identified by dots, and shows that there was some correlation between azimuth error and Doppler spread. The correlation coefficient is only 0.42 but is significant; the probability of this arising from independent variables is less than one percent. If we were to limit the measurements of azimuth to times when the Doppler spread was less than 0.4 Hz, we would eliminate all spread-F returns and limit the RMS error in azimuth to a maximum of about 0.7 degrees. However a slight increase in the Doppler-spread limit above 0.4 Hz would greatly increase the maximum RMS error.

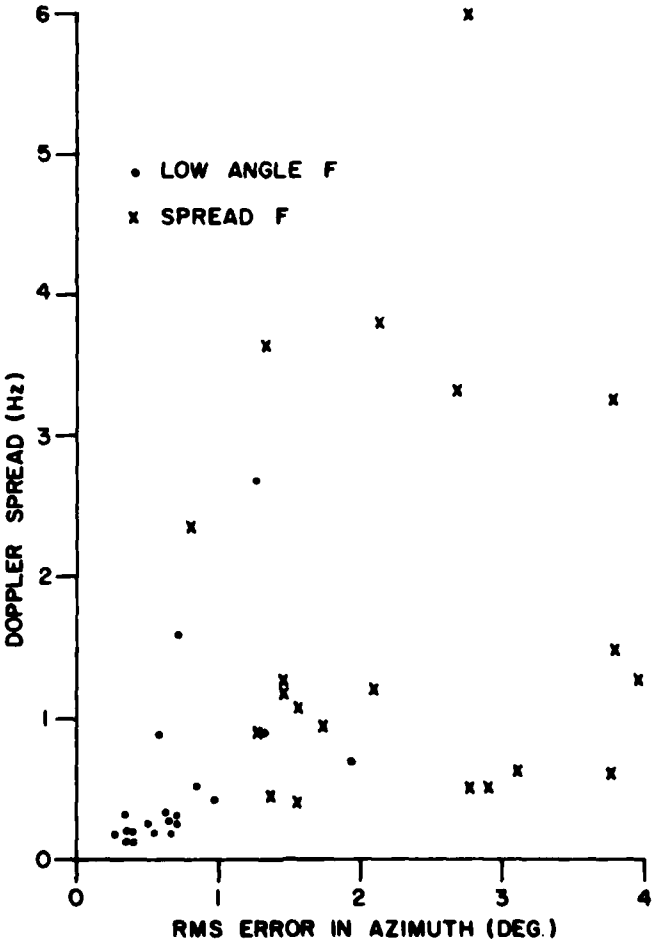

Figure 11. Doppler-Spread vs RMS Azimuth Error for F Mode

Figure 11 shows mean Doppler spread averaged over approximately 30-minute periods against RMS error averaged over the same period. If Doppler spread were used as a selection criterion in an operational system it would be done on an individual measurement basis, but the basic principle, that low Doppler spread indicates a good azimuth estimate, should still apply.

The measurement of Doppler spread does not require that absolute Doppler be determined. However, it does require a Doppler resolution of a small fraction of a Hz. The transmitted signal must have one or more discrete lines in its spectrum. These could be the carrier in an amplitude-modulated transmission or modulation lines in a digital transmission. Some signals such as single-sideband suppressed carrier or signals from an unstable transmitter may not satisfy this requirement.

An added benefit of the Doppler spread criterion is that interference from undesired signals, whose presence in the final bandwidth of the system leads to angle errors, will also cause an increase in apparent Doppler spread and therefore be discriminated against.

4.1.2 Scan-by-Scan Analysis

A scan-by-scan method of azimuth estimation using an RMS phase-deviation criterion to select scans for azimuth averaging was described in Section 3.1.2. The AZPLT6 program which performs this estimation was tested on the fixed-frequency signals from this experiment.

Histograms of the averaged scan-by-scan results are shown in Figures 12 to 15 along with the single-mode histograms for the same period derived from the swept-frequency data as in Section 4.1.1.

Figure 12 is intended mainly as a reference. Only one mode, the two-hop sporadic-E mode was present at the time, and mode intereference would not have been a problem, except possibly where two or more paths existed within the one mode. Thus we would not expect much difference between the Scan-by-Scan results (lower histogram) and the "mode separated" results from the swept-frequency data (upper histogram). One additional factor must be taken into account, however, in comparing the two histograms. The swept frequency analysis used data from a one-second interval, while the scan-by-scan analysis used data from a five-second interval. Therefore, if the errors were uncorrelated over a period of one second, and if they were stationary and unbiased, we would expect the errors in the swept-frequency estimates to be $\sqrt{5}$ or 2.24 times as large as those in the fixed-frequency estimates. This value should be an upper bound on the ratio of the errors for the two cases, and since it is very unlikely that the above conditions existed, we would expect the ratio to fall well below the value of 2.24 but above unity. The RMS error over the period of the histogram is printed on each histogram, and we see that, for the data of Figure 12, the ratio of RMS error for the swept frequency data to that of the fixed frequency data is 1.36. This indicates that the conditions specified above were not well satisfied. The RMS error for the swept-frequency case would have been somewhat lower if the two occurrences at 7.5° and 8° had not existed, and the small sample size means that these may well have had more effect on the RMS error calculation than they should have had. The remaining part of the histogram is very similar to that for the scan-by-scan case, leading us to wonder if the ratio of 1.36

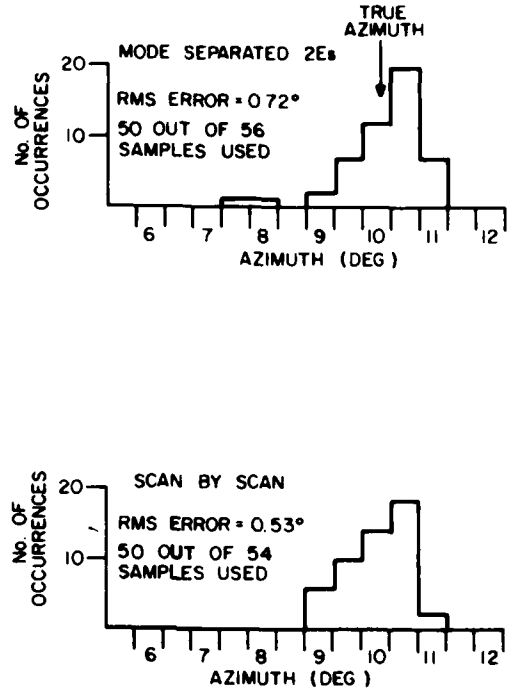

Figure 12. Histograms for Day 342 2:48 to 3:55 Single Mode only Present

is a somewhat high estimate of the effect of the difference between the two sample times. In any case, it seems certain that this ratio will vary with conditions, but should be generally in the range between unity and two, probably closer to unity.

The number of samples shown on the histogram refers to those which passed the phase-linearity tests, and which were included in the histograms, and the number of samples that were available for testing. In the case of the scan by scan analysis, a sample passed the test if 20 out of 64 scans had RMS phase deviations less than 80 degrees and 15 degrees for arrays 1 and 2 respectively. The large percentage passing the tests in Figure 12 indicates that the signal was mainly single-moded.

Figure 13 shows histograms for a two and a half hour period when two modes, sporadic E in one and two-hop paths, were present. The scan-by-scan histogram indicates much lower errors than do the two single-mode histograms. The RMS error ratio between the scan by scan data and the best single mode is 1.8, near the maximum expected. This indicates that the scan by scan method has done as well as would be possible from the best single mode. Only about one half of the scan-by-scan results satisfied the test, probably because the amplitudes of the two modes were nearly equal. But even fewer of the single-mode results were acceptable. This may have been due to the relatively low amplitude of both modes.

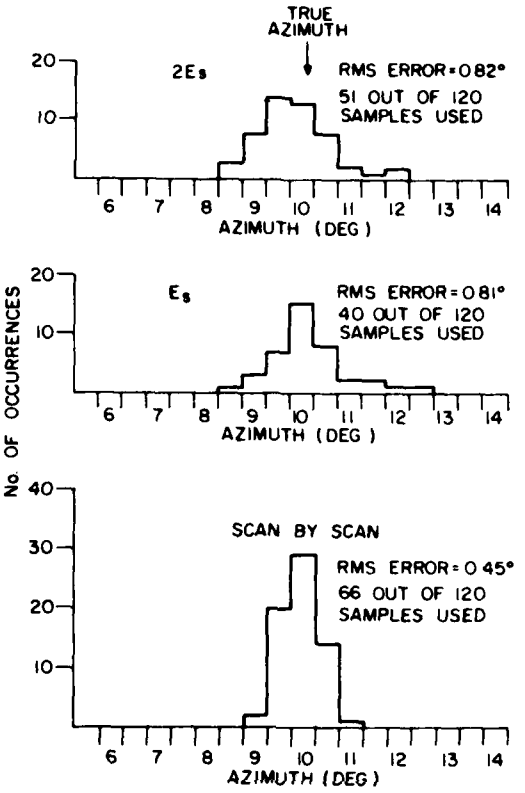

Figure 13. Histograms for Day 331 20:40 to 22:39 Es and 2Es Modes Present – Both Weak

The histograms of Figure 14 are also for a two-mode case, but this time for high-and low-angle F modes. The low-angle mode is somewhat stronger than the high-angle one. The scan-by-scan error is again lower than that of the best single mode. This time the RMS-error ratio is 1.9, about as high as might be expected, indicating that the scan-by-scan method is working very well. The conditions here were somewhat more favourable for the scan-by-scan method than the conditions of Figure 13 since one mode was considerably stronger than the other, and that mode was the more accurate. The unequal amplitudes of the two modes is probably the major cause of the fact that all samples of the scan-by-scan data passed the acceptance test.

A more severe test of the method is illustrated in Figure 15, when three modes were present, two of them about equal in amplitude and the third somewhat weaker. Actually some extremely weak two-hop sporadic E was also present for part of the time but was too weak to give any swept frequency results. Conditions were rather bad, with some range spreading of the modes and as can be seen from Figure 15, the accuracy of all the modes was poor. However the scan-by-scan results are still quite useable. The RMS-error ratio for the best mode (the weakest) was 1.36 and for the better of the two stronger modes was 1.46. This is about as good as could be expected, considering the bias of about one degree in the results which would reduce the possible improvement for the long duration considerably. About 73% of the

scan-by-scan estimates were acceptable, an encouraging result for such poor conditions.

The above results were selected to illustrate a number of different conditions, and are considered typical. They represent over six hours of measurement. Many other data were analyzed in the same way and the results are summarized in Figure 16 which shows histograms of all the error ratios found. The abscissa represents the ratio of RMS error for a separated mode to that for the scan-by-scan analysis. Each occurrence represents a measurement over a period of roughly one to three hours. The upper histogram indicates cases where only one mode was present, the middle one indicates the ratios for the strongest of multiple modes and the lower one indicates the ratios for the most accurate of multiple modes (which can be the same as the strongest). No cases were found where the ratio for the strongest mode was less than one, and only one case was found where the ratio for the most accurate mode was less than one. In this latter case the most accurate mode, the two-hop sporadic-E mode, was very much weaker than the heavily spread F mode, which had an RMS error of 3.49°. With this one exception these ratios fall within the expected range. The histograms for strongest mode and most accurate mode are very similar, mainly because the strongest mode was usually the most accurate in these data. This will not always be the case, however, particularly where normal E and F modes occur at the same time. Experience from other experiments with shorter path lengths has shown that the F mode is usually stronger and usually less accurate. Under such conditions we would expect the stronger mode to dominate in the scan-by-scan analysis and the errors should be similar to those of the strongest separated mode.

The error ratio tends to be a little lower for the case where only one mode is present. This seems to indicate that the scan-by-scan method works better when there is more than one mode, an unlikely result. A more likely explanation is that this is just a statistical variation resulting from the rather small sample size and that the extra modes really do not improve the results but also do very little harm other than reducing the number or rate of accepted measurement values.

We can conclude that the phase linearity test applied to scan-by-scan analysis is a useful technique for reducing the azimuth estimate errors, and that the resulting errors are about as low as we would get from the strongest mode alone, if it could be separated. Where two or more modes exist with nearly equal amplitudes, the main effect is a reduction in the rate of acceptable azimuth estimates.

4.1.3 Weighted-Mean Method

The weighted-mean method described in Section 3.1.1 was tested on the recorded data. Histograms were plotted for the same time periods as were used for the scan-by-scan analysis, but only one (Figure 17) is presented here along with a table (Table 1) comparing RMS errors for this method with those for the scan-by-scan method. The weighted-mean method used the same 5-second record of data as the scan-by-scan method and should therefore be directly comparable to it. Table 1 shows that the weighted-mean method gives slightly larger errors. Figure 17 may be compared with Figure 13 which covers the same time period. Although the RMS error for the weighted-mean

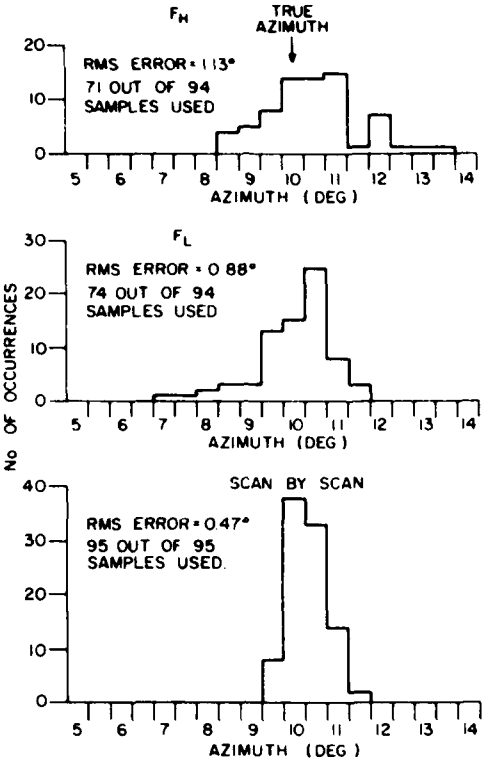

Figure 14. Histograms for Day 330 11:12 to 13:15 Strong FL and Moderate FH Present

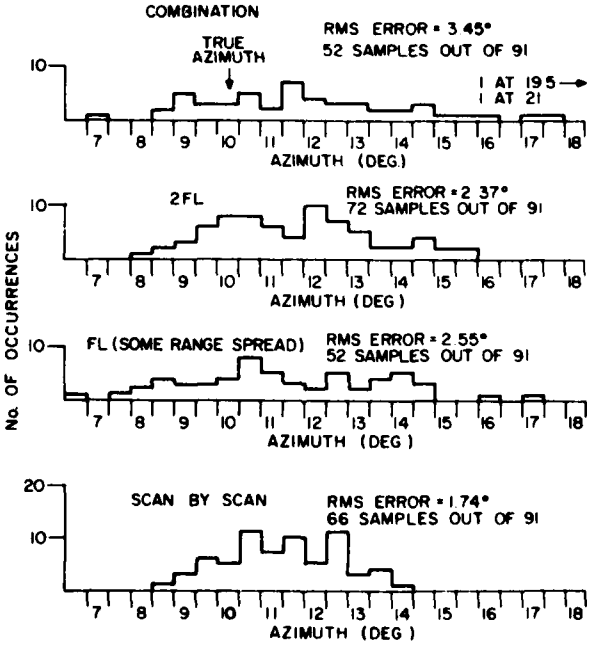

Figure 15. Histograms for Day 341 8:25 to 10:19 FL, Combination and 2 FL Modes Present

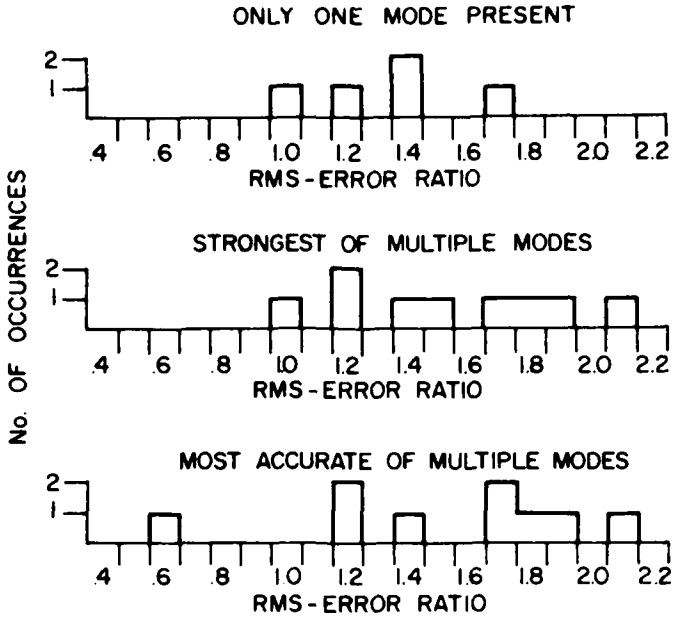

Figure 16. Histogram of Ratios of RMS Error for Separated Modes to RMS Error for Scan by Scan Technique

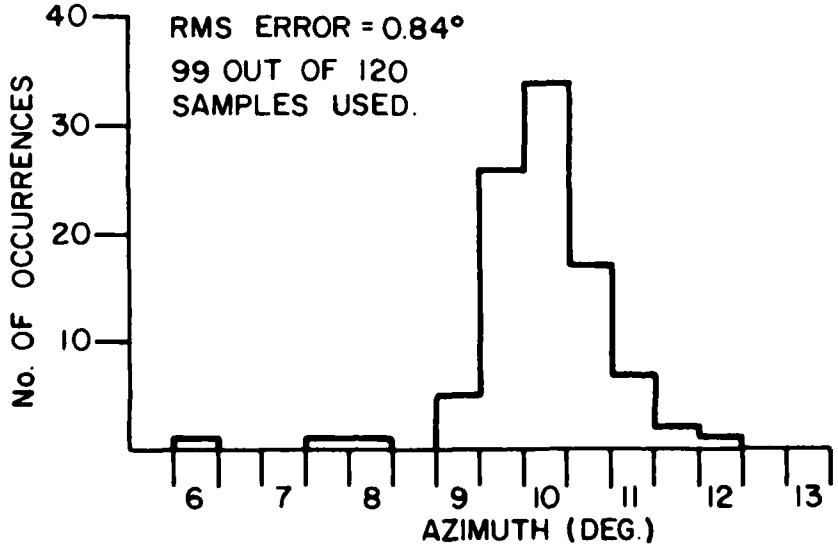

Figure 17. Histogram of Azimuth Estimates for Weighted Mean Technique Day 331 20:04 – 22:39

method was almost twice that for the scan-by-scan method, this deviation is strongly influenced by a few extreme points. Ninety-nine of 120 estimates were accepted, a somewhat higher ratio than that for other histograms. The main portion of the histogram looks nearly as good as that for the scan-by-scan method and better than those for the separate modes. As can be seen in Table 1, the example of Figure 17 had the worst ratio of RMS error relative to the scan-by-scan method of all the time periods. The average ratio is about 1.3.

TABLE 1

Comparison of RMS Errors for the Scan-by-Scan and Weighted-Mean Methods

Modes Present	Doppler Spread (Hz)	RMS Error (Deg) Scan by Scan S	Weighted Mean W	Ratio W/S
F_L, F_H	0.18	0.38	0.43	1.13
F_L	0.21	0.57	0.58	1.02
F_L, F_H	0.34	0.71	0.87	1.23
F_L, $2F_L$, Comb.	0.44	1.74	2.14	1.23
F_L $2F_L$	0.54	0.85	1.35	1.59
2Es	0.59	0.53	0.68	1.28
Spread F	1.04	2.96	3.64	1.23
F_L, F_H	1.07	0.72	1.16	1.61
F_L	1.08	0.82	1.01	1.23
Es, 2Es	1.25	0.45	0.84	1.87
Es	1.53	0.23	0.27	1.17
2Es	1.67	1.08	1.20	1.11
F_L, F_H	1.67	0.48	0.77	1.60
F_L, F_H	2.65	0.68	0.78	1.15
2Es, Spread F	4.33	2.49	3.97	1.59

However, the weighted-mean method is a more complex method than the scan-by-scan method, and should be capable of separating modes to some extent by means of their differences in Doppler. Results of a test of this method on a Sept Iles-Ottawa path which is a shorter path (911 km) and does not pass through the auroral zone were more encouraging[4]. The poorer performance on the longer path appears due to the different characteristics of the paths. The parameters used for the method in the present experiment were the same as those used for the shorter path and probably were not optimum for this path.

The Frobisher-Ottawa path is a more dynamic one. Changes occur over shorter time intervals and Doppler spreads are greater. Thus the five-second integration time of the Fourier transform may be too long.

The Sept-Iles-Ottawa path usually had normal one-hop E and F modes with the F mode generally stronger. This is where the weighted-mean method has a high potential. It can make use of the weaker but more accurate E mode. The E mode would receive more weight because of its lower elevation angle and lower RMS phase deviation; the amplitude weight was not a very strong one. On the other hand the scan-by-scan method is always influenced much more by the stronger mode. On the Frobisher-Ottawa path the sporadic-E mode did not often coincide in time with the F modes. Multiple modes generally consisted of one-hop and two-hop Es with the one hop usually stronger and more accurate, or of low-angle F and other F modes with the low-angle mode almost always stronger and more accurate. Thus the stronger mode was usually more accurate, an ideal condition for the scan-by-scan method.

4.2 Analysis of Some Spread-F Reflections

The results of Section 4.1.1 have indicated that very large errors result in direction-finding measurements when propagation is by spread-F reflections. It is the intention of this Section to investigate in more detail the characteristics of these reflections. A number of cases of spread-F reflections (well spread in range with little evidence of high and low-angle structure) were selected and analyzed with the AZEL3 program to provide azimuth and elevation estimates for the Doppler cells with highest amplitude and low RMS phase deviation. Results were used, for a particular Doppler cell only if the RMS phase deviations were not greater than 30 degrees for array 1, and 15 degrees for array 2. Results were also discarded if the elevation angle was less than 7 degrees, to eliminate any returns from the E region. For each five-second record up to ten azimuths and elevations, each from a different Doppler cell, could be found although usually much fewer than ten would pass the tests. These were plotted as points on azimuths vs Doppler and elevation-vs-Doppler scatter plots, together with data from other times within some time interval selected for the desired conditions.

Figures 18 and 19 are examples of this type of plot for a case where the Doppler Spread was relatively low. The low spread is due in part to the low transmitted frequency, since, for a given velocity of the reflection point, the Doppler is proportional to frequency; but even after taking this into account the Doppler spread is quite low in this case compared to that found for the average spread-F conditions. The spread in azimuth corresponds to a reflection area width of about 400 km. From Figure 18 the points can be seen to be distributed fairly uniformly both in Doppler and in azimuth, but

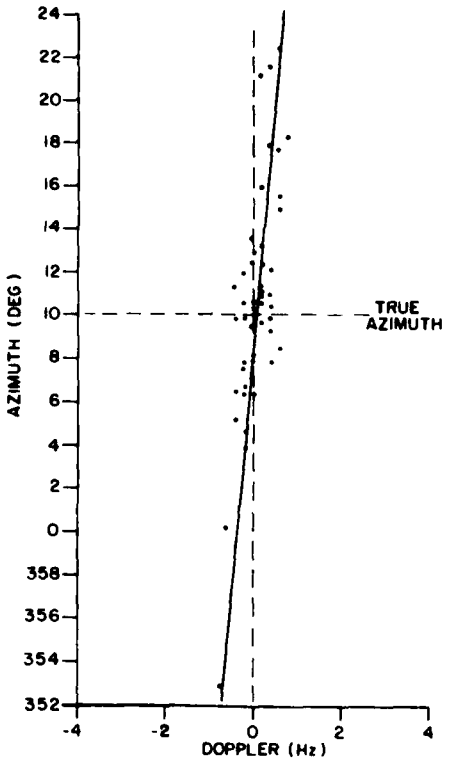

Figure 18. Scatter Plot – Azimuth vs Doppler – Day 332 20:09 - 21:06
Spread-F Conditions, Freq. = 5.14 MHz

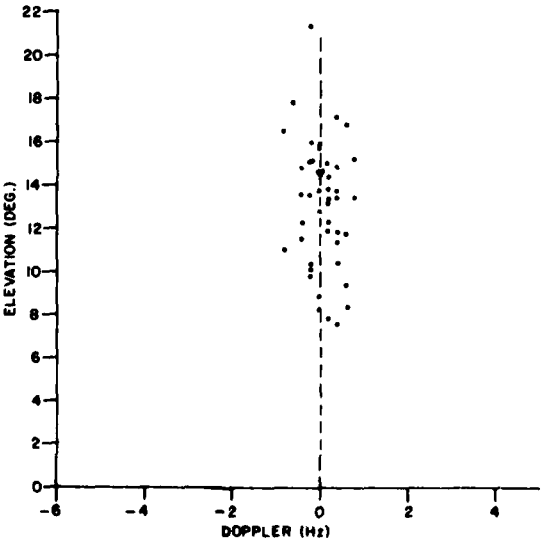

Figure 19. Scatter Plot – Elevation vs Doppler – Day 332 20:09 - 21:06
Spread-F Conditions, Freq. = 5.14 MHz

with some correlation between the two. The correlation coefficient of the 49 points was found to be 0.72. According to the Students t-distribution, the probability that independent variables would give this correlation with this number of sample points is less than 0.01 percent. Thus we must conclude that the Doppler and azimuth are correlated. A least-squares linear fit to the points, with azimuth taken as the independent variable, has been drawn as a dashed line in Figure 18. It has a slope of 21 degrees per Hz, which is consistent with a general motion of the reflecting points from right to left (as seen by the receiver) with a velocity component at right angles to the path, from east to west, of about 300 km/hr. This estimate may be a little low since the computation of the slope assumed the azimuth variable had no error. Since the Doppler spread was small in this case, the effect on the slope of the azimuth errors could have been significant.

The elevation-vs-Doppler plot of Figure 19 indicates a spread, about a central value of 13 degrees, which may result from an extended reflection area of about 500 km along the path. Figure 19 does not show the correlation between elevation and Doppler that would be expected from a north-south component of velocity over the extended area. Therefore the velocity is likely restricted to a near E-W direction.

The picture suggested by these plots is that of a rough medium providing reflections over an area with a radius of about 200 km. The reflecting points appear to be moving in an east-to-west direction with a fairly uniform velocity of about 300 km/hr., and not much turbulence. Of course, the motion may be a wave motion rather than a general bulk motion of the medium. A simple simulation, using a rippled-mirror model of an ionospheric wave with a 200 km wavelength and 20 km wave amplitude, gave results similar to those of Figure 19 when the wave was moved across the receiving path with a velocity of 380 km/hr. It is difficult to distinguish between wave motion and bulk motion from these measurements.

Figures 20 and 21 show the results for another day at a slightly higher frequency. The Doppler spread is greater, but the azimuth-Doppler correlation coefficient is only about 0.30. However this is high enough to be significant (the probability of this value resulting from independent variables is less than one percent). The linear least-squares fit (azimuth taken as independent variable) to the points of Figure 20 is shown as a dashed line. It has a slope of 11 degrees per Hz, which implies a velocity component of about 400 km/hr across-path from east to west. There is a bias of about two degrees in azimuth. No significant correlation exists in Figure 21 indicating a lack of along-path (north-south) motion.

We conclude then, that reflections occurred over some rough patch centred about 2 degrees (about 40 km) to the west of the direct great-circle path and that there was some type of turbulent motion which caused Doppler spreading. There appears to have been an overall motion of the reflection points from east to west although it was somewhat masked by the turbulence. The extent of the reflecting patch was smaller, especially across-path, than that of the first example. The bias in the azimuth was probably due to a gradient in electron density in the across-path direction as a result of some difference in the production or loss of electrons, or as a result of a wave-like disturbance propagating through the medium. The offset is in the

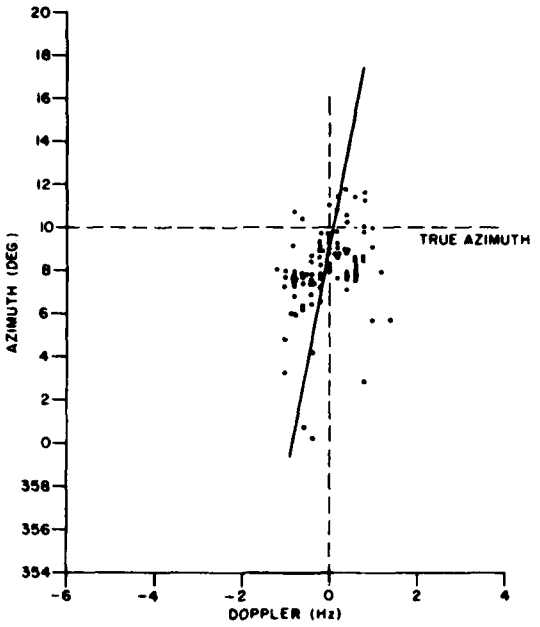

Figure 20. Scatter Plot -- Azimuth vs Doppler -- Day 333 20:04 - 20:29 Spread-F Conditions, Freq. = 6.69 MHz

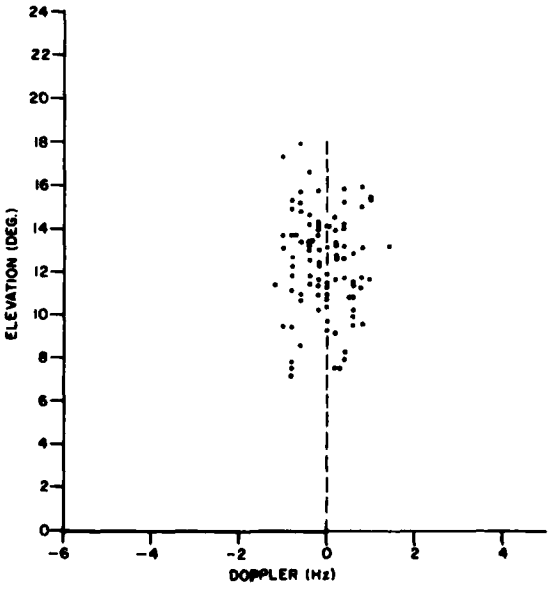

Figure 21. Scatter Plot -- Elevation vs Doppler -- Day 333 20:04 -20:29 Spread-F Conditions, Freq. = 6.69 MHz

direction which would be expected for the sunset-caused gradient, but the time of the measurement is about three hours after sunset at that height.

Figures 22 and 23 show a case where the Doppler spread was even higher and the bias in azimuth was even greater. The angular spreads seem somewhat less than those of the previous examples however, and the elevation angle is centred at a lower value than before. The lower elevation angles could be due to a displacement of the reflecting area from the mid-point away from the receiver, or simply to a lower virtual height. No correlation is evident in either figure.

A fourth rather unusual case of spread-F propagation was analyzed in a different way. Extremely large elevation angles were found which were much too high for normal F-mode low-angle propagation. At the same time the measured ranges were not consistent with high-angle propagation or multiple hops. A plot of azimuth vs Doppler showed an off-path bias of about 1.5 degrees, not too surprising after some of the previous examples.

The strange elevation angle characteristics were investigated by plotting elevation angle vs range delay from the swept-frequency recordings in the same way as elevation-vs-Doppler plots were done from the fixed-frequency recordings. The results for two time periods about an hour apart are shown in Figures 24 and 25. A very definite dependence of elevation angle on range was found in both cases and lines were drawn "by eye" to represent these trends. Then, using simple geometry, based on a curved earth and point reflections, ranges and elevation angles were computed for various virtual reflection heights and positions of the reflection point along the path. This latter was defined by the distance on the earth's surface from the point directly below the reflection point to the receiver. First, a virtual height was picked, and then the elevation angle and range were computed for a trial distance. The resulting point was then compared to the experimental line and a new distance picked to bring the point closer to the line. This process was repeated until the point fell very close to the line. Then a new height was selected and the whole process repeated. The result is a group of points marked with x's in Figures 24 and 25. The numbers in the brackets next to the points indicate the virtual height and distance from the reflection point to the receiver. Thus these numbers represent samples of the reflection point positions which would be necessary to give the "average" results of the experimental data.

These points are plotted in Figure 26 to give a locus of reflection points on a height-versus-distance map. Of course the measured points of reflection are scattered about these lines.

It is not clear whether the difference between the two time intervals results from the time difference or from the frequency difference, and it is also not clear what the cause of the strong dependence between height and distance is. Since the ground distance between transmitter and receiver is 2108 km, the reflection area is seen to be very far from the mid-point (the distance to the transmitter is more than twice the distance to the receiver). The reflection patch is over 50 km long at any one time or frequency, and about 40 km wide, and is offset about 20 km to the west of the great-circle path. During the first time-period a normal low-angle-F mode also existed, but this disappeared before the second time period. It appears that gradients occurred

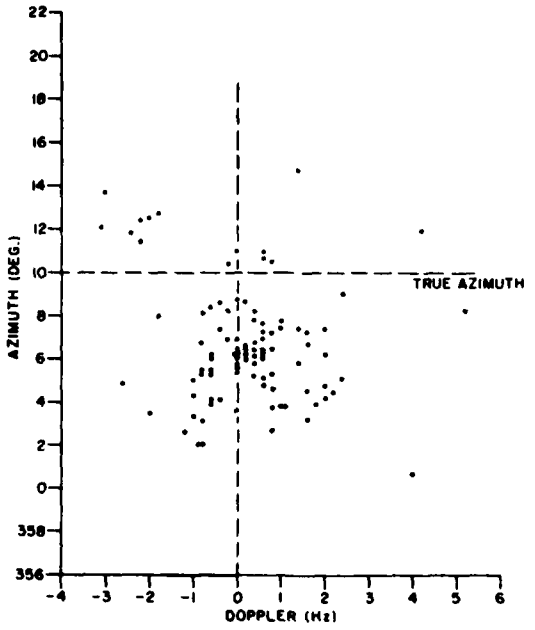

Figure 22. Scatter Plot – Azimuth vs Doppler – Day 339 02:16 - 02:55 Spread-F Conditions, Freq. = 8.25 MHz

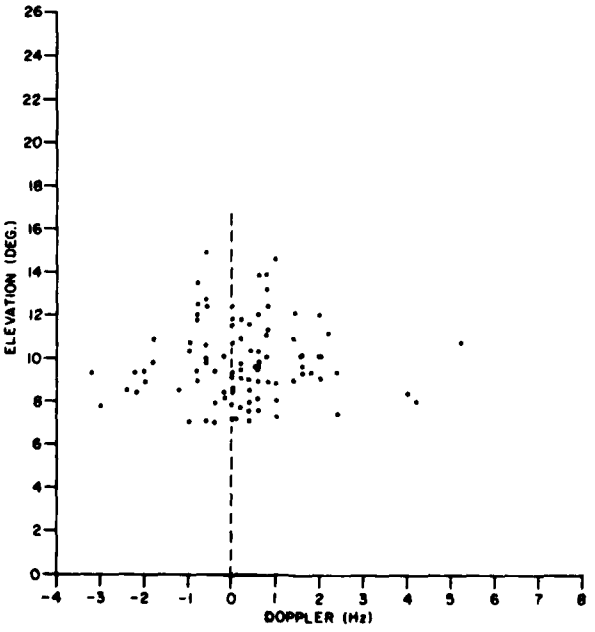

Figure 23. Scatter Plot – Elevation vs Doppler – Day 339 02:16 -02:55 Spread-F Conditions, Freq. = 8.25 MHz

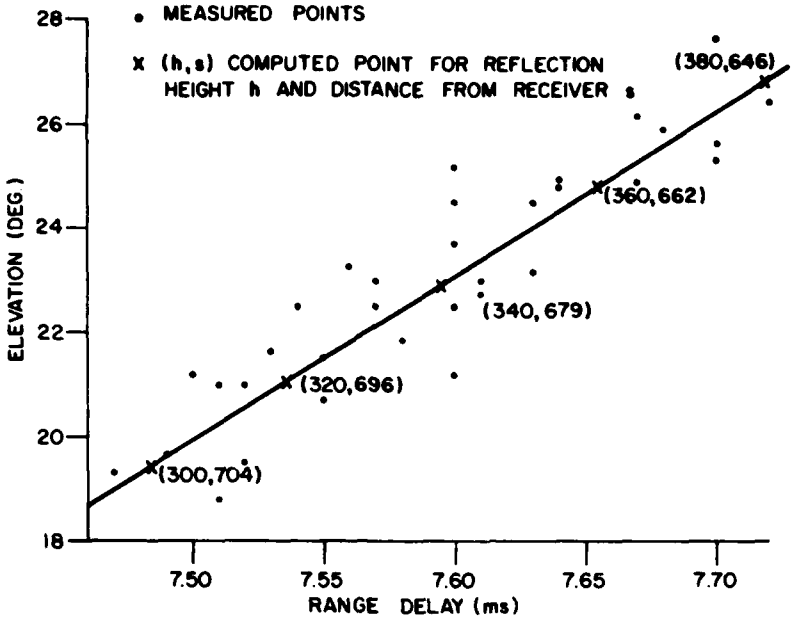

Figure 24. Scatter Plot – Elevation vs Range – Day 331 15:36 - 15:58
Freq. = 14 MHz

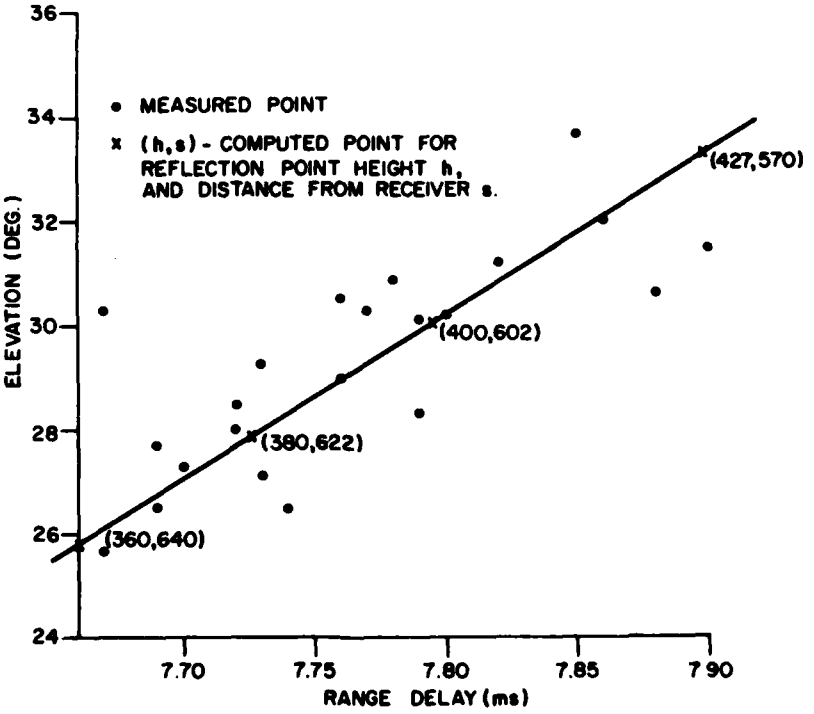

Figure 25. Scatter Plot – Elevation vs Range – Day 331 16:38 - 16:59
Freq. = 10.6 MHz

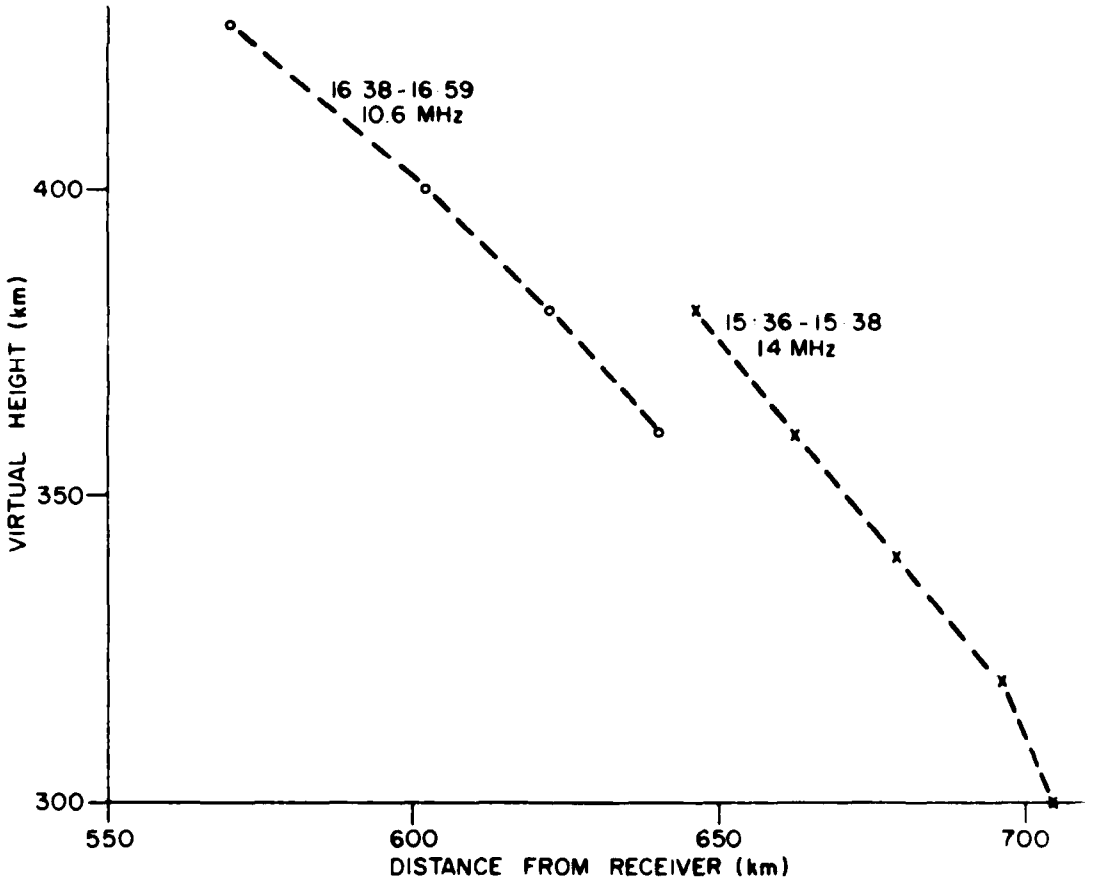

Figure 26. Reflection Point Virtual Height vs Ground Distance from Receiver Day 331

in the electron density in both the along-path (north-south) direction and the across-path direction. The north-south gradient must have been very strong.

The above interpretation of the data is based on a simple model of the ionosphere with reflections from points. These points are only virtual points which give the correct delays and angles of arrival. The true path may not correspond too well to the one computed from the model, and different interpretations may be possible.

These examples give an indication of the conditions which can exist for paths like the Frobisher-Ottawa one, which traverse the auroral zone. These spread-F modes are characterized by large Doppler spreads, large azimuth and elevation-angle spreads, and often, large biases in the azimuth and elevation angles. There is also evidence of overall motion of the reflection points either by bulk motion of the medium or by waves propagating through it.

Some idea of the percentage of time these spread-F conditions occur on the path can be obtained from Figures 2 and 3. It is apparent that it is a

significant percentage, and since very poor angle estimates are provided by these conditions, they can be a serious problem. At least some of the time that spread-F conditions exist an E mode exists as well, and if these modes can be separated the problem will not be so serious.

5. SUMMARY AND DISCUSSION

The measurements reported here were made around the first of December 1976 over a path whose ground length was about 2100 km and whose mid-point was in the auroral zone. Propagation conditions were, on the average, somewhat more disturbed than those typically observed on lower-latitude paths. Large spreads in Doppler and range delay for a given mode occurred relatively frequently. Spread in range for F-mode propagation was always accompanied by a spread in angle-of-arrival in both the azimuth and elevation dimensions. On the other hand, large Doppler spreads did not always mean poor angular accuracy.

Separation of modes by range discrimination with one-second swept-frequency transmissions provided information on the errors to be expected from various modes. All the E-mode propagation appears to have been sporadic, often with relatively high Doppler spread. However the one-hop sporadic-E mode proved to be a very accurate mode, giving RMS azimuth errors with a median value of about 0.4 degrees. The two-hop mode was not as good, having a median RMS error of about one degree.

Low-angle F-mode propagation, if single hop and not spread in range, provided reasonable accuracy with only a small percentage of RMS azimuth errors greater than one degree and a median value of about 0.7 degrees. Under the same conditions, the high-angle F mode gave about the same result with possibly marginally higher errors. When the F mode was spread in range or had multiple hops (including combination with E mode), the errors were high, with median values of two degrees or more. Spread-F conditions existed a significant percentage of the time and appear to be a serious problem for direction finding on this type of path.

The above-mentioned values of RMS error are for one-second records. The range processing, which is a Fourier transformation, effectively integrates the data over the one-second period, and so produces a one-second average of the angle measurement. The use of longer records would presumably reduce the RMS error to some degree.

This method of range discrimination cannot of course be used in an operational system since it requires the cooperation of the transmitter. A proposed method of estimating azimuth which does not have this requirement is the scan-by-scan method which computes a mean value of azimuth based on a large number of samples (scans across the array). Samples are used in the averaging only if the RMS phase deviations across each array are below specified values. This is equivalent to a test for planarity of the phase front. Tests of this scan-by-scan method on the data from this experiment indicate that it gives about as good results as could be expected from the single mode with highest accuracy. It should be noted however that the conditions on this path are well suited to the scan-by-scan method which relies

mainly on the strongest mode. For this path the strongest mode was almost always also the most accurate. This will not always be the case for other paths of different lengths at different latitudes.

Another method of azimuth estimation proposed in an earlier report[4], and referred to here as the weighted-mean method, provided an accuracy not quite as good as that of the scan-by-scan method. The weighted-mean method, which used Doppler processing in an attempt to separate modes, is a more complex method and was expected to provide higher accuracy than the scan-by-scan method. Its failure to do so may be a result of the fact that the parameters selected for weighted-mean method were probably not optimum for this path. Also it appears that the relatively dynamic nature of the propagation conditions and the particular combination and relative amplitude of modes favoured the scan-by-scan method. This main strength of the weighted-mean method is that it can make use of the weaker mode when it is the more accurate, and this was rarely the case in this experiment.

On shorter and lower-latitude paths with simultaneous normal E and F modes, it is believed that the weighted-mean method would be the superior one.

6. ACKNOWLEDGEMENTS

In the development of methods and computer programs for the analysis of the data for this report, extensive use was made of previous work by Dr. D.W. Rice of Communications Research Centre.

This work was supported by the Department of National Defence, Canada.

7. REFERENCES

1. Rice, D.W. and E.L. Winacott, *A Sampling Array for HF Direction-Finding Research*, CRC Report No. 1310, Communications Research Centre, Department of Communications, Ottawa, November 1977.

2. Hayden, E.C., *Propagation Studies Using Direction-Finding Techniques*, Journal of Research of the National Bureau of Standards, D, Radio Propagation, Volume 65D, No. 3, pp. 197-212, May-June, 1961.

3. Rook, B.J., *Study of the Behaviour and Stability of Phase Fronts on Short Time Scales*, CRC Report No. 1312, Communications Research Centre, Department of Communications, February 1978.

4. Venier, G.O., *An Experiment to Investigate the Value of Doppler Shift Measurement as a Means of Improving Wide Aperture HFDF Azimuth Estimates* (U), CRC Technical Note No. 688, Communications Research Centre, Department of Communications, Ottawa, November 1977. RESTRICTED.

5. Rice, D.W., G.O. Venier, and G. Atkinson. *The Effect of Signal Modulation in the Application of a Wave-Front Linearity Test in HF Direction-Finding*, Proceedings of the 1978 NRL-ONR Symposium on the Effect of the Ionosphere on Space and Terrestrial Systems, Arlington, VA, January 24-26, 1978, paper 3-12.

APPENDIX A

Formulas for Computation of Weights in the Weighted-Mean Method

The weight given to the azimuth computed for i^{th} Doppler cell is:

$$W_i = Ge_i \cdot Gd_i \cdot Ga_i,$$

where

Ge_i, Gd_i and Ga_i are "quality" factors depending on elevation angle, RMS phase deviation across the arrays and received power, respectively in the i^{th} cell. They are described below.

$$Ge_i = \exp\,[(2.0-\theta e_i)/5.0] \qquad \text{for } \theta e_i > 2.0$$

$$= 1 \qquad \theta e_i \leq 2.0,$$

where

θe_i is the elevation angle in degrees in the i^{th} cell.

$$Gd_i = \exp\{[20.0-(d_{1i}+2.0d_{2i})]/7.0\} \qquad \text{for } d_{1i}+2.0d_{2i}>20.0$$

$$= 1 \qquad \text{for } d_{1i}+2.0d_{2i}\leq 20.0$$

where

d_{1i} and d_{2i} are the RMS phase deviations in degrees across arrays 1 and 2 respectively in the i^{th} Doppler cell.

$$Ga_i = V_i/Vs,$$

where

V_i is the received voltage magnitude in the i^{th} cell, and
V_s is the sum of the voltage magnitudes over all Doppler cells used in the computation.

The overall weight for the weighted mean azimuth is given by:

$$W_o = W_s \cdot \exp(\sigma_d/0.1) \cdot \exp(\sigma_b/0.50)$$

where

W_s is the sum of weights for all the Doppler cells used in the computations,
σ_d is the standard deviation of Doppler frequency in Hz across the cells, and
σ_b is the standard deviation of bearing in degrees across the cells.

For the results presented here an overall weight threshold of 10^{-5} was used. Estimates whose weights were less than this were discarded.